



1 A Comparative Study to Reveal the Influence of Typhoons on the 2 Transport, Production and Accumulation of O₃ in the Pearl River 3 Delta, China

4 Kun Qu^{1,2}, Xuesong Wang^{1,2}, Yu Yan^{1,2}, Jin Shen³, Teng Xiao^{1,2}, Huabin Dong^{1,2}, Limin Zeng^{1,2}, and
5 Yuanhang Zhang^{1,2,4,5}

6 ¹State Key Joint Laboratory of Environmental Simulation and Pollution Control, College of Environmental Sciences and Engineering,
7 Peking University, Beijing 100871, China

8 ²International Joint Laboratory for Regional Pollution Control, Ministry of Education, Beijing, 100816, China

9 ³State Key Laboratory of Regional Air Quality Monitoring, Guangdong Key Laboratory of Secondary Air Pollution Research, Guangdong
10 Environmental Monitoring Center, Guangzhou 510308, China

11 ⁴Beijing Innovation Center for Engineering Science and Advanced Technology, Peking University, Beijing 100871, China

12 ⁵CAS Center for Excellence in Regional Atmospheric Environment, Chinese Academy of Sciences, Xiamen 361021, China

13 Correspondence to: Xuesong Wang (xswang@pku.edu.cn) and Yuanhang Zhang (yhzhang@pku.edu.cn)

14 **Abstract.** The Pearl River Delta (PRD) region in South China is faced with severe ambient O₃ pollution in autumn and summer,
15 which mostly coincides with the occurrence of typhoons above the Northwest Pacific. With increasingly severe O₃ pollution
16 in the PRD under the influence of typhoons, it is necessary to gain a comprehensive understanding of the impact of typhoons
17 on O₃ transport, production and accumulation for efficient O₃ reduction. In this study, we analysed the general influence of
18 typhoons on O₃ pollution in the PRD via systematic comparisons of meteorological conditions, O₃ processes and sources on
19 O₃ pollution days with and without typhoon occurrence (denoted as the typhoon-induced and no-typhoon scenarios,
20 respectively), and also examined the differences in these influences in autumn and summer. The results show that the approach
21 of typhoons was accompanied by higher wind speeds and strengthened downdrafts in autumn as well as the inflows of more
22 polluted air masses in summer, suggesting favourable O₃ transport conditions in the typhoon-induced scenario in both seasons.
23 However, the effect of typhoons on the production and accumulation of O₃ were distinct. Typhoons led to reduced cloud cover,
24 and thus stronger solar radiation in autumn, which accelerated O₃ production, but the shorter residence time of local air masses
25 was unfavourable for the accumulation of O₃ within the PRD. In contrast, in summer, typhoons increased cloud cover, and
26 weakened solar radiation, thus restraining O₃ formation, but the growing residence time of local air masses favoured O₃
27 accumulation. The modelling results using the Community Multiscale Air Quality (CMAQ) model for the typical O₃ pollution
28 days suggest increasing contributions from the transport processes as well as sources outside the PRD for O₃ pollution,
29 confirming enhanced O₃ transport under typhoon influence in both seasons. The results of the process analysis in CMAQ
30 suggest that the chemical process contributed more in autumn but less in summer in the PRD. Since O₃ production and
31 accumulation cannot be enhanced at the same time, the proportion of O₃ contributed by emissions within the PRD was likely
32 to decrease in both seasons. The difference in the typhoon influence on O₃ processes in autumn and summer can be attributed
33 to the seasonal variation of the East Asian monsoon. From the “meteorology-process-source” perspective, this study revealed



34 the complex influence of typhoons on O₃ pollution in the PRD and their seasonal differences. To alleviate O₃ pollution under
35 typhoon influence, emission control is needed on a larger scale, rather than only within the PRD.

36 **1 Introduction**

37 Tropospheric ozone (O₃) serves as a secondary pollutant in ambient air and is detrimental for human health and crop
38 production (Wang et al., 2017; Liu et al., 2018; Mills et al., 2018). Ambient O₃ is produced from its precursors, i.e., nitrogen
39 oxides (NO_x = NO + NO₂) and volatile organic compounds (VOCs), through chemical reactions in the presence of sunlight.
40 This O₃ can accumulate locally, or be transported to downwind regions. Under unfavourable meteorological conditions,
41 enhanced transport, production and/or accumulation of O₃ can all contribute to the O₃ pollution within a region (National
42 Research Council, 1991).

43

44 As the largest city cluster in South China, the Pearl River Delta (PRD) region is faced with frequent ambient O₃ pollution,
45 especially in autumn and summer (Li et al., 2014; Wang et al., 2017; Lu et al., 2018). Along with the continuous increasing of
46 O₃ levels in recent years (Li et al., 2019), O₃ has become the primary contributor to the deterioration of air quality in this
47 region (Feng et al., 2019). The occurrence of O₃ pollution in the PRD is predominantly related to the influence of typhoons
48 (or tropical cyclones) above the Northwest Pacific (Gao et al., 2018; Deng et al., 2019; Lin et al., 2019). According to Gao et
49 al. (2018), seven out of the nine most severe O₃ episodes (regional-mean maximum 8-h average O₃ concentrations of > 240
50 µg/m³) during 2014–2016 coincided with the approach of typhoons. The changes in the track and intensity of typhoons may
51 contribute to the growing trend of O₃ levels recently and in future (Lam, 2018; Lam et al., 2018). Therefore, a
52 comprehensive understanding of the influence of typhoons on the transport, production and accumulation of O₃ has
53 important implications for efficient and strategic O₃ reduction in the PRD.

54

55 Analyses of typhoon-related O₃ episodes in the PRD have been extensively reported in previous publications. The effect of
56 typhoons on O₃ pollution is closely linked to meteorological conditions that are conducive to the transport, production and/or
57 accumulation of O₃. Stagnation caused by typhoons, characterised by low wind speeds, has been reported during many
58 episodes, and it promotes the accumulation of locally formed O₃ within the PRD (Wang et al., 1998; So and Wang, 2003;
59 Wang and Kwok, 2003; Huang et al., 2005; Lam et al., 2005; Jiang et al., 2008; Zhang et al., 2014; Chow et al., 2019).
60 Strong north or west winds were observed or simulated during several episodes, suggesting the potentially strengthened
61 transport of pollutants under typhoon influence (Wang et al., 2001; Yang et al., 2012; Wang et al., 2015; Wei et al., 2016).
62 Downdrafts on the outskirts of typhoons may promote downward O₃ transport and contribute to near-ground O₃ pollution as
63 well (Lam, 2018), but its appearance in the PRD has only been examined in a few studies. Cloudless conditions and strong
64 solar radiation enhance O₃ production, which is another important cause of O₃ pollution (Wang et al., 1998; Wang and
65 Kwok, 2003; Li et al., 2018; Yue et al., 2018; Chow et al., 2019). In a more direct way, several studies have utilised



66 chemical transport models, along with the Process Analysis (PA) tool and source apportionment (SA) methods, to quantify
67 and compare the contributions of various O₃ processes (e.g., transport and the chemical process) and sources (e.g., local
68 emissions, outside emissions and background) during these episodes. Based on reports by Huang et al. (2005), Lam et al.
69 (2005), Jiang et al. (2008), Wang et al. (2010), Li (2013), Wang et al. (2015), Wei et al. (2016) and Chen et al. (2018),
70 horizontal/vertical transport and chemical production may both be the main contributing process for typhoon-induced O₃
71 pollution in different parts of the PRD. The SA results revealed that emissions within the PRD contributed 40–80% of O₃
72 during typhoon-related O₃ episodes (Li et al., 2012; Li, 2013; Chen et al., 2015), suggesting the potentially important role of
73 O₃ accumulation for O₃ pollution here. However, despite massive episode-based studies, several important questions still
74 remain: Are O₃ transport, production and accumulation within the PRD all enhanced at the same time by typhoons? Do both
75 O₃ pollution seasons (autumn and summer) experience similar impact of typhoons on O₃ pollution? More thorough
76 investigations are needed to answer these questions.

77

78 In this study, we present systematic comparisons between O₃ pollution in the typhoon-induced and no-typhoon scenarios
79 (definitions given in Sect. 2.2) to elucidate the influence of typhoons on O₃ transport, production and accumulation in the PRD
80 and to reveal their seasonal differences. October and July in 2014–2018 were selected as the representative months for autumn
81 and summer, respectively. Multiple datasets, including the ERA-Interim re-analysis, the routine monitoring datasets,
82 trajectories calculated by the Hysplit model and the modelling results of typical O₃ pollution days using the Community
83 Multiscale Air Quality (CMAQ) model, were used in the comparisons. A detailed introduction of these datasets is presented
84 in Sect. 2. The comparisons were conducted from the perspectives of meteorological conditions (Sect. 3), O₃ processes and
85 sources (Sect. 4), and the conclusions about the influence of typhoons on the causes of ambient O₃ pollution in the PRD in the
86 two seasons are illustrated in Sect. 5.

87 **2 Methods**

88 **2.1 Datasets**

89 The detailed information for the datasets utilised in the comparison of meteorological conditions is presented below:

- 90 • **Re-analysis datasets:** We mainly used the ERA-Interim re-analysis product in the analyses due to its more available
91 parameters and high spatial coverage (available at [https://www.ecmwf.int/en/forecasts/datasets/reanalysis-datasets/era-](https://www.ecmwf.int/en/forecasts/datasets/reanalysis-datasets/era-interim)
92 interim, last accessed: March 2020; Dee et al., 2011; Berrisford et al., 2011). Specifically, meteorological parameters
93 used in the comparisons include the following three categories: (1) near-surface parameters from the analysis fields,
94 including air temperature (at a height of 2 m), relative humidity (RH, at 1000 hPa), horizontal wind speeds (at a height
95 of 10 m; zonal and meridional wind speeds were also involved in the comparisons), and low (for the height at which
96 pressure/surface pressure > 0.8), medium (for the height at which 0.45 < pressure/surface pressure < 0.8), high (for the
97 height at which pressure/surface pressure < 0.45) and total cloud covers; (2) near-surface parameters from the forecast



98 fields, including plenary boundary layer (PBL) height and net surface solar radiation; and (3) upper air parameters at
99 multiple heights, including horizontal and vertical wind speeds, cloud water content and O₃ mixing ratio. The focus of
100 this study is O₃ pollution during the daytime, and therefore, only the parameters at 14:00 local time (LT) were selected
101 for the analyses (except for net surface solar radiation, which was averaged within 8:00–17:00 LT).

- 102 • **Surface meteorological routine monitoring datasets:** The routine monitoring meteorological data collected at 29
103 national meteorological sites within the PRD (locations shown in Fig. S1a) were also used to explore the
104 meteorological features under the impact of typhoons. The parameters include air temperature, RH, and wind speed and
105 direction (also transformed to zonal and meridional wind speeds in the comparisons) at 14:00 LT.
- 106 • **Typhoon information:** The times, locations and intensities of typhoons were provided by the Chinese Meteorological
107 Administration Best Track Dataset of tropical cyclones (Ying et al., 2014). The tracks of all typhoons that potentially
108 contributed to O₃ pollution in the PRD during the study period (October and July in 2014–2018) are shown in Fig. S2
109 and S3.
- 110 • **O₃ concentrations:** Hourly O₃ concentration data, which were originally released by the China National Environmental
111 Monitoring Centre, were downloaded from <http://beijingair.sinaapp.com> (last accessed: Dec. 2018). Based on the
112 hourly data, we calculated the maximum 1-hr concentrations (MDA1) and maximum 8-hr average concentrations
113 (MDA8) of O₃ in nine municipalities in the PRD (including Guangzhou, Shenzhen, Zhuhai, Foshan, Jiangmen,
114 Zhaoqing, Huizhou, Dongguan and Zhongshan) to identify O₃ pollution days that served as samples in the comparisons.

115 2.2 Definition and classification of O₃ pollution days

116 In this study, O₃ pollution days were defined as the days when the MDA1 exceeds 200 µg/m³ or the MDA8 exceeds 160
117 µg/m³ for O₃ (both are the Grade-II thresholds of the Chinese National Ambient Air Quality Standard (NAAQS), GB 3095–
118 2012) in any of the nine municipalities in the PRD. According to these criteria, there were 78 and 55 O₃ pollution days
119 (given in Table S1 and S2) during October and July in 2014–2018, respectively. The information about these O₃ pollution
120 days in the two representative months is listed in Table 1 (overall) and S3 (monthly), including the numbers of days, their
121 proportions in the month, and the corresponding mean O₃ concentrations (MDA8 and MDA1, highest values among nine
122 municipalities in the PRD). Although there were more O₃ pollution days in October than in July, O₃ pollution days under
123 typhoon influence accounted for ~30% of all days in both months. Higher O₃ MDA1 and MDA8 values can be generally
124 found with the appearance of typhoons in comparison with days without typhoons, further indicating the important role of
125 typhoons in O₃ pollution in the PRD.

126

127 The differing locations of typhoons can result in the diverse effect of typhoons on O₃ pollution (Chow et al., 2018). To
128 determine the general influence of typhoons on O₃ pollution in the PRD, it was necessary to further select O₃ pollution days
129 coinciding with typhoons with similar directions and distances from the PRD. First, we removed five O₃ pollution days in
130 July with typhoons located to the due north or southwest of the PRD from the analyses. As is shown in Fig. 1, the remaining

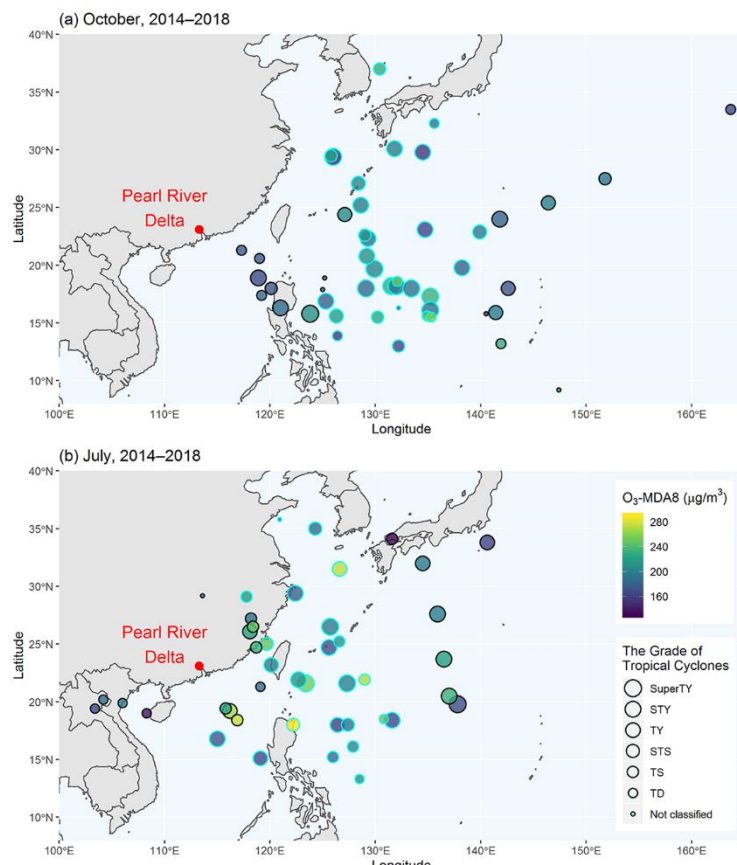


131 days, including all O₃ pollution days in October and most O₃ pollution days in July under typhoon influence, were associated
132 with typhoons to the east of the PRD, which were more likely to cause O₃ pollution (Chow et al., 2018). After this, based on
133 the distances between typhoon centres and the PRD (at 14:00 LT), we classified the pollution days in each season into three
134 categories: close typhoon (lowest 20% of distances), typhoon (20–80% intervals of distances), and far typhoon (longest 20%
135 of distances)-induced days. The typhoon-induced days represent O₃ pollution days with general typhoon influence, and they
136 were compared with those without the appearance of typhoons (hereafter denoted as the no-typhoon days). It should be noted
137 that the distances between typhoon centres and the PRD on the typhoon-induced days were overall larger in autumn (1400–
138 2800 km, at 14:00 LT) than in summer (700–2000 km, at 14:00 LT), which may be the consequence of the different
139 characteristics of typhoon paths in the two seasons: most typhoons in autumn travel northwest initially and then turn
140 northward in the areas east of the Philippines (Fig. S2), whereas they are more likely to end up landing in Southeast China in
141 summer (Fig. S3). Since the influence of typhoons on O₃ pollution may be different when typhoons come close enough to
142 the PRD (Lam et al., 2005; Li, 2013), the close typhoon-induced days were considered to be a special scenario in the
143 comparisons of meteorological conditions (Sect. 3.5). Owing to the less apparent effect of typhoons over the PRD, we did
144 not include the far typhoon-induced days in the discussions.

145

146 **Table 1.** The numbers and proportions of O₃ pollution days, and O₃ concentrations for various scenarios.

Parameter	October, 2014–2018	July, 2014–2018
Number (proportion) of O ₃ pollution days	78 (50.3%)	55 (35.5%)
With typhoons	49 (31.6%)	45 (29.0%)
Typhoon-induced days	30 (19.4%)	24 (15.5%)
Close typhoon-induced days	10 (6.5%)	8 (5.2%)
Without typhoons (no-typhoon days)	29 (18.7%)	10 (6.5%)
Mean PRD-max O ₃ MDA8 ($\mu\text{g}/\text{m}^3$)		
With typhoons	195.0	205.3
Typhoon-induced days	199.5	205.4
Close typhoon-induced days	184.6	225.7
Without typhoons (no-typhoon days)	189.8	187.8
Mean PRD-max O ₃ MDA1 ($\mu\text{g}/\text{m}^3$)		
With typhoons	230.4	259.8
Typhoon-induced days	235.2	260.0
Close typhoon-induced days	219.2	277.1
Without typhoons (no-typhoon days)	231.5	246.5



147

148 **Figure 1.** The location and intensity of typhoons at 14:00 LT on all O₃ pollution days with typhoons, and the corresponding O₃ MDA8
149 concentrations (maximum values in the nine municipalities of the PRD) on the same days during (a) October and (b) July in 2014–2018.
150 The points with cyan borders indicate the “typhoon-induced” O₃ pollution days used in the comparisons. The grades of tropical cyclones
151 (Chinese National Standard, GB/T 19201-2006) are as follows: SuperTY - super typhoon; STY - severe typhoon; TY - typhoon; STS -
152 severe tropical storm; TS - tropical storm; TD - tropical depression; others are grouped as “not classified”.

153 **2.3 Calculation of the trajectories and air parcel residence time**

154 To explore the potential effect of cross-regional transport on O₃ pollution in the PRD, we applied the Hysplit model (Stein et
155 al., 2015) with the Global Data Assimilation System (GDAS) datasets as inputs to calculate 72-h backward trajectories reaching
156 the PRD at 14:00 LT for all O₃ pollution days. The Modiesha site (23.1 °N, 113.3 °E; Fig. S1b), which is located in the central
157 part of the PRD, was the endpoint of backward trajectories, with its height set as 500 m above the ground.

158

159 Air parcel residence time (APRT), discussed by Huang et al. (2019), is the average number of hours that air parcels originated
160 from one place stay within a pre-defined domain, and long APRTs can be used to indicate good accumulation conditions for
161 locally sourced pollutants. To calculate APRTs in the PRD, we designed a 21×15 point matrix that embraces the whole PRD
162 (Fig. S4), and forward trajectories starting from these points were also calculated using the Hysplit model. The height of all



163 points was set as 100 m above the ground, which is close to the height of emissions. The start times were set as 2:00, 8:00,
164 14:00 and 20:00 LT for all O₃ pollution days. Afterwards, the length of time each trajectory remained within the administration
165 borders of the PRD, i.e., APRT, was calculated. The APRT values of all points were averaged for each scenario and were
166 interpolated to obtain field results.

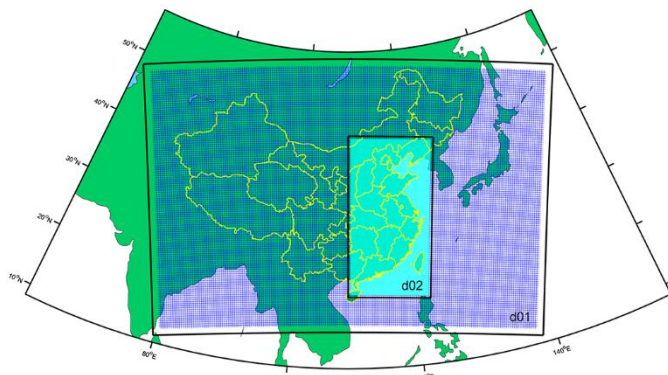
167 **2.4 CMAQ modelling: basic setups and modelling methods**

168 We utilised the widely used 3D chemical transport model, the CMAQ model (version 5.0.2), to investigate the effect of
169 typhoons on O₃ processes and sources. October 2015 and July 2016 featured the most severe O₃ pollution under typhoon
170 influence among all representative months of the two seasons (Table S3), and thus, they were chosen as the period in the
171 CMAQ modelling (because there was no severe O₃ pollution during the first 10 days of October 2015 and 3–5 November can
172 be classified as the no-typhoon O₃ pollution days, we adjusted the modelling period in autumn to 11 October–10 November
173 2015) and all O₃ pollution days in these two months served as representative O₃ pollution days under multiple scenarios. In
174 detail, there were four typhoon-induced O₃ pollution days (14–16 and 21 October 2015) and four no-typhoon O₃ pollution days
175 (28 October and 3–5 November 2015) in October 2015, whereas there were four and six typhoon-induced and no-typhoon
176 days in July 2016, respectively (typhoon-induced: 7–8 and 30–31 July 2016; and no-typhoon: 22–26 and 29 July 2016). The
177 results of the daytime (9:00–17:00 LT) O₃ PA and SA on the above O₃ pollution days were averaged for each scenario and
178 were used in the comparisons.
179

180 The main setups of the CMAQ modelling are presented as follows. Two-nested modelling domains with the resolutions of 36
181 and 12 km (denoted as d01 and d02, respectively) were set in this study (Fig. 2). Specifically, d02 covers the whole East and
182 Central China (EC-China), enabling us to evaluate the contribution of emissions in these areas to O₃ pollution in the PRD.
183 There were 19 vertical layers in the CMAQ modelling, with about 10 layers within the PBL (about 0–1 km in heights; Guo et
184 al., 2016). The Weather Research and Forecasting (WRF) model (version 3.2) provided the meteorological fields used as inputs.
185 SMOKE (version 2.5) and MEGAN (version 2.10) were used to process the anthropogenic and biogenic emission files,
186 respectively. The anthropogenic emission inventory used in this study consisted of the following three parts: (1) emissions in
187 the PRD, which were provided by the Guangdong Environmental Monitoring Centre; (2) emissions in other areas of mainland
188 China, which were extracted from the MEIC inventory (He, 2012); and (3) emissions in other countries and regions in Asia,
189 which were extracted from the MIX inventory (Li et al., 2017). The initial and boundary conditions of the d01 modelling were
190 obtained from the same-period results of the MOZART-4 global model (available at <https://www.acom.ucar.edu/wrf-chem/mozart.shtml>, last accessed: Dec. 2019), and those of the d02 modelling were extracted from the d01 modelling results.
191 The SAPRC07 gas-phase chemistry mechanism (Carter, 2010) and the AERO6 aerosol scheme were set in the CMAQ
192 modelling. In addition, the simulations of the two months were both started 10 days ahead to minimise the disturbance of the
193 bias of the initial conditions. The modelling performances of CMAQ and WRF were determined to be acceptable based on the
194 comparisons between the observational and modelling series of meteorological parameters, O₃ MDA8, daily NO₂

196 concentrations and the mixing ratios of non-methane hydrocarbons (NMHCs) in the PRD (for details, refer to Sect. 1 of the
197 Supplement Information), which ensures the validity of the further analyses.

198



199

200 **Figure 2.** Two-nested modelling domain, noted as d01 and d02. The black boxes indicate the WRF modelling domains, and the nested
201 areas are the CMAQ modelling domains.

202 The PA tool in CMAQ was implemented to quantify the hourly contributions of O₃ processes (or integrated process rate, IPR),
203 which includes vertical/horizontal transport (convection+diffusion), chemical process (net O₃ production), dry deposition and
204 cloud process. To explore the overall effect of typhoons on O₃ transport and production in the region, the mean PA results
205 within the administration boundaries of the PRD were calculated and compared.

206

207 We used the classic Brute Force Method (BFM) to identify the contributions of emissions (including anthropogenic and
208 biogenic emissions) in the PRD and other regions in the d02 (mainly EC-China), as well as regions outside the d02 (the
209 boundary conditions of the d02) for O₃ pollution in the PRD (hereafter denoted as the contributions of PRD, EC-China and
210 BCON, or *S_{PRD}*, *S_{EC-China}* and *S_{BCON}*, respectively). For a pollutant, the contribution of a specific emission, E_i, can be calculated
211 in two ways: (1) the difference between the modelled concentrations of the base case (all emissions involved) and the sensitivity
212 case where E_i is zeroed out (i.e., top-down BFM); (2) the difference between two sensitivity cases where emissions expect E_i
213 and all of the emissions are zeroed out, respectively (i.e., bottom-up BFM). Owing to the non-linearity between O₃ and its
214 precursors, biases may occur between the results of two types of BFM methods (Clappier et al., 2017). Therefore, the average
215 of the top-down and bottom-up BFM results was treated as the quantified contributions of the concerned sources. Four
216 simulation cases were run in this study, including (the modelled O₃ concentration in each case was also marked in brackets):

- 217 • the base case (*C_{base}*);
218 • the PRD-cut case (*C_{PRD_cut}*), where emissions within the PRD were zeroed out;
219 • the PRD-only case (*C_{PRD_only}*), where emissions outside the PRD (within d02) were zeroed out; and
220 • the zero-emission case (*C₀*), where all emissions within the d02 were zeroed out.



221 Afterwards, the S_{PRD} , $S_{EC-China}$ and S_{BCON} values (in concentrations) in the polluted areas of the PRD (where modelled daytime
222 O₃ concentrations > 160 µg/m³, the Grade-II O₃ MDA8 thresholds of the Chinese NAAQS) were calculated using the following
223 equations,

$$S_{PRD} = \frac{1}{2}[(C_{base} - C_{PRD_cut}) + (C_{PRD_only} - C_0)], \quad (R1)$$

$$S_{EC-China} = \frac{1}{2}[(C_{base} - C_{PRD_only}) + (C_{PRD_cut} - C_0)], \quad (R2)$$

$$S_{BCON} = C_0. \quad (R3)$$

224 The percentage forms of these values were used in the comparisons.

225 3 Comparison of meteorological conditions

226 3.1 Overview: comparison of meteorological parameters in the PRD

227 First, we compared near-ground meteorological parameters in the PRD on the typhoon-induced and no-typhoon O₃ pollution
228 days. The parameters from the ERA-Interim re-analysis (including the parameters of the first and second categories in Sect.
229 2.1) and the routine monitoring datasets (including air temperature, RH, wind speed, zonal and meridional wind speeds)
230 were used in the comparison. The Mann-Whitney U test was applied to determine whether the above parameters were
231 significantly different ($p < 0.05$) in the two types of O₃ pollution scenarios.

232

233 As is listed in Table 2, statistically significant differences between the typhoon-induced and no-typhoon scenarios existed for
234 most of the parameters, such as meridional (south-north) wind speed, cloud covers within various height ranges and net
235 surface solar radiation — in both seasons, these parameters were significantly different for the two scenarios. It indicates that
236 the causes of O₃ pollution may vary on typhoon-induced and no-typhoon O₃ pollution days. Note that air temperature, one of
237 the parameters most closely related to O₃ pollution in the PRD (Zhao et al., 2019), was not significantly different in the two
238 scenarios. We also found that the comparison in autumn and summer did not produce the same results: the typhoon-induced
239 days in autumn featured lower RH, stronger winds (especially north wind), reduced cloud cover (low, medium, high and
240 total) and stronger surface solar radiation, whereas in summer, these days had higher RH, weaker south winds, more cloud
241 cover (medium, high and total), weaker surface solar radiation and lower PBL heights. Therefore, the impact of typhoons on
242 O₃ pollution differs in the two seasons, as well. In order to reveal the impact of typhoons on O₃ transport, production, and
243 accumulation in the PRD, more detailed comparisons of the corresponding meteorological indicators are presented in the
244 following sections.



245 **Table 2.** The comparisons of meteorological parameters (all at 14:00 LT except for net surface solar radiation, which is the average value
 246 for 9:00–17:00 LT) in the PRD for the three scenarios (no-typhoon, typhoon-induced, close typhoon-induced) in two seasons (autumn,
 247 summer). RM, routine measurement; ERA, ERA-Interim re-analysis. All of the parameters are presented as “the mean value \pm standard
 248 deviation”. The differences between parameters in the typhoon-induced or close typhoon-induced scenarios and the corresponding
 249 typhoon-induced scenarios for the same season are given in parentheses, and “*” indicates $p < 0.05$, or statistically significant differences
 250 between these parameters when the Mann-Whitney U test is used.

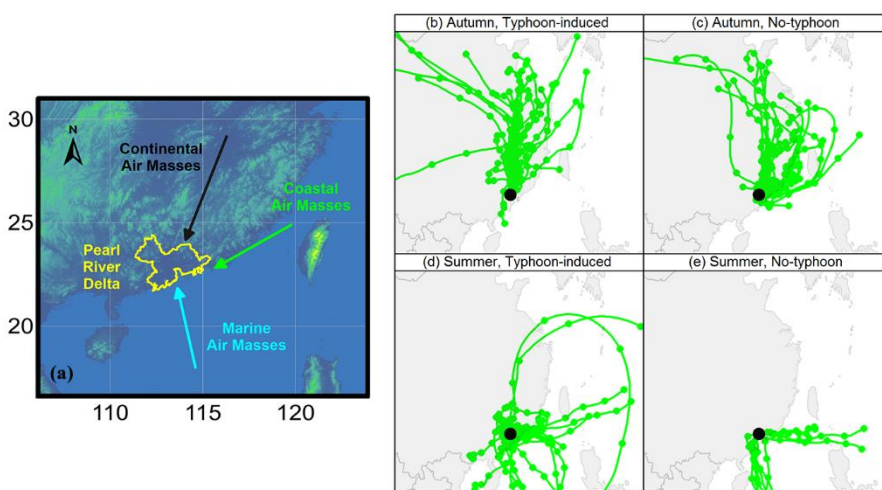
Parameters	Data Source	Autumn (October, 2014–2018)			Summer (July, 2014–2018)		
		No-typhoon	Typhoon-induced	Close Typhoon-induced	No-typhoon	Typhoon-induced	Close Typhoon-induced
Air Temperature (°C)	RM	29.1 \pm 2.2	29.3 \pm 1.8 (+0.2)	29.6 \pm 1.5 (+0.5, *)	33.7 \pm 2.0	33.9 \pm 2.0 (+0.2)	35.0 \pm 1.5 (+1.3, *)
	ERA	29.2 \pm 2.1	29.3 \pm 1.6 (+0.1)	29.6 \pm 1.5 (+0.4, *)	33.4 \pm 1.8	33.5 \pm 1.4 (+0.1)	34.6 \pm 1.4 (+1.2, *)
RH (%)	RM	52.4 \pm 10.2	44.8 \pm 10.4 (-7.6, *)	51.4 \pm 12.4 (-1.0)	57.0 \pm 9.3	58.3 \pm 9.7 (+1.3)	56.9 \pm 6.4 (-0.1)
	ERA	54.0 \pm 9.8	48.3 \pm 11.2 (-5.7, *)	52.2 \pm 12.4 (-1.8, *)	62.6 \pm 10.8	66.4 \pm 9.4 (+3.8, *)	62.5 \pm 9.4 (+0.1)
Wind Speed (m/s)	RM	2.33 \pm 1.18	2.58 \pm 1.23 (+0.25, *)	2.96 \pm 1.40 (+0.63, *)	2.46 \pm 1.33	2.30 \pm 1.20 (-0.16)	2.53 \pm 1.16 (+0.07)
	ERA	2.39 \pm 1.30	2.54 \pm 0.99 (+0.15, *)	3.53 \pm 1.11 (+1.14, *)	2.41 \pm 0.99	2.18 \pm 1.18 (-0.23, *)	2.61 \pm 1.05 (+0.20)
Zonal (East-West) Wind Speed (m/s)	RM	-0.83 \pm 1.72	-0.59 \pm 1.70 (+0.24, *)	-0.13 \pm 1.74 (+0.70, *)	-0.41 \pm 2.05	-0.03 \pm 1.94 (+0.38)	0.73 \pm 1.98 (+1.14, *)
Meridional (South-North) Wind Speed (m/s)	RM	-0.36 \pm 1.74	-1.49 \pm 1.66 (-1.13, *)	-2.21 \pm 1.66 (-1.85, *)	0.79 \pm 1.69	0.01 \pm 1.72 (-0.78, *)	-0.69 \pm 1.68 (-1.48, *)
ERA	-0.27 \pm 1.82	-1.97 \pm 1.16 (-1.70, *)	-3.27 \pm 1.29 (-3.00, *)	1.61 \pm 1.09	0.64 \pm 1.58 (-0.97, *)	-0.68 \pm 1.19 (-2.29, *)	
Low Cloud Cover (%)	ERA	17.2 \pm 22.7	4.2 \pm 11.9 (-13.0, *)	15.5 \pm 23.9 (-1.7, *)	8.7 \pm 9.4	7.1 \pm 9.5 (-1.6, *)	5.2 \pm 5.0 (-3.5, *)
Medium Cloud Cover (%)	ERA	22.2 \pm 26.5	10.4 \pm 19.7 (-11.8, *)	9.5 \pm 14.5 (-12.7, *)	8.7 \pm 11.1	15.4 \pm 15.1 (+6.7, *)	21.5 \pm 15.5 (+12.8, *)
High Cloud Cover (%)	ERA	12.1 \pm 23.1	7.2 \pm 16.3 (-4.9, *)	34.6 \pm 35.6 (+22.5, *)	32.2 \pm 30.0	44.9 \pm 29.3 (+12.7, *)	51.0 \pm 34.2 (+18.8, *)
Total Cloud Cover (%)	ERA	43.5 \pm 32.3	20.5 \pm 25.7 (-23.0, *)	51.9 \pm 33.1 (+8.4, *)	43.7 \pm 26.7	58.3 \pm 22.7 (+14.6, *)	67.5 \pm 21.0 (+23.7, *)
Net Surface Solar Radiation (W/m ²)	ERA	456.9 \pm 78.4	516.6 \pm 66.7 (+59.7, *)	516.5 \pm 62.8 (+59.6, *)	560.3 \pm 93.1	523.2 \pm 74.4 (-37.1, *)	541.9 \pm 54.0 (-18.4, *)
PBL Height (m)	ERA	1471 \pm 315	1473 \pm 348 (+2)	1349 \pm 227 (-122, *)	1268 \pm 383	1037 \pm 289 (-231, *)	1196 \pm 300 (-72, *)

251 3.2 O₃ transport conditions: comparison of wind speeds, backward trajectories and vertical air motions

252 The higher wind speeds and/or O₃ levels in the transported air masses are, the more likely O₃ transport plays an increasingly
 253 important role in O₃ pollution. In the PRD, O₃ levels are closely linked to the type of air masses influencing the region, which
 254 can be identified based on backward trajectories. According to Zheng et al. (2010), there are generally three types of air masses

that are transported into the PRD along different paths and contribute to O₃ pollution here, namely, the continental, coastal and marine air masses (Fig. 3a). The continental and coastal air masses can bring O₃ from EC-China to the PRD, and thus, they are typically recognised as being polluted and contributing to relatively high O₃ levels in the PRD. In contrast, the marine air masses, originated from the South China Sea, are much cleaner. In this section, we studied the influence of typhoons on O₃ transport by comparing wind speeds and 72-h backward trajectories in various scenarios.

260



261

262 **Figure 3.** (a) Three O₃ transport paths towards the PRD. (b–e) Backward trajectories at 14:00 LT for the four scenarios: (b) autumn,
263 typhoon-induced; (c) autumn, no-typhoon; (d) summer, typhoon-induced; and (e) summer, no-typhoon. The black dots indicate the end
264 point of all trajectories, i.e., where the Modiesha site in the central PRD is located.

265 As is displayed in Fig. 3b–c, we identified the influence of continental air masses on the typhoon-induced O₃ pollution days
266 in autumn, as well as mixed contributions from the continental and coastal air masses on the corresponding no-typhoon days.
267 However, for the former scenario, significantly increased wind speeds (Table 2) ensure more favourable conditions for the
268 transport of O₃. In summer, the three types of air masses may all have affected O₃ pollution in the typhoon-induced scenario,
269 while only the marine air masses influenced the PRD in the no-typhoon scenario (Fig. 3d–e). Since wind speeds did not vary
270 significantly (Table 2), the inflows of much more polluted air masses resulted in that typhoons also tended to increase the
271 contribution of transport to O₃ pollution in the PRD in summer. In addition, the influence of different air masses was also
272 accompanied with variations in the prevailing winds in the PRD, that is, north winds and easterlies in the typhoon-induced and
273 no-typhoon scenario in autumn, respectively, and southwest winds in the no-typhoon scenario in summer (indicated by wind
274 roses in Fig. S5). For the typhoon-induced scenario in summer, the dominate wind direction is hard to determine. These
275 variations in the local wind fields potentially result in the different spatial distribution of O₃ concentrations in various scenarios.
276

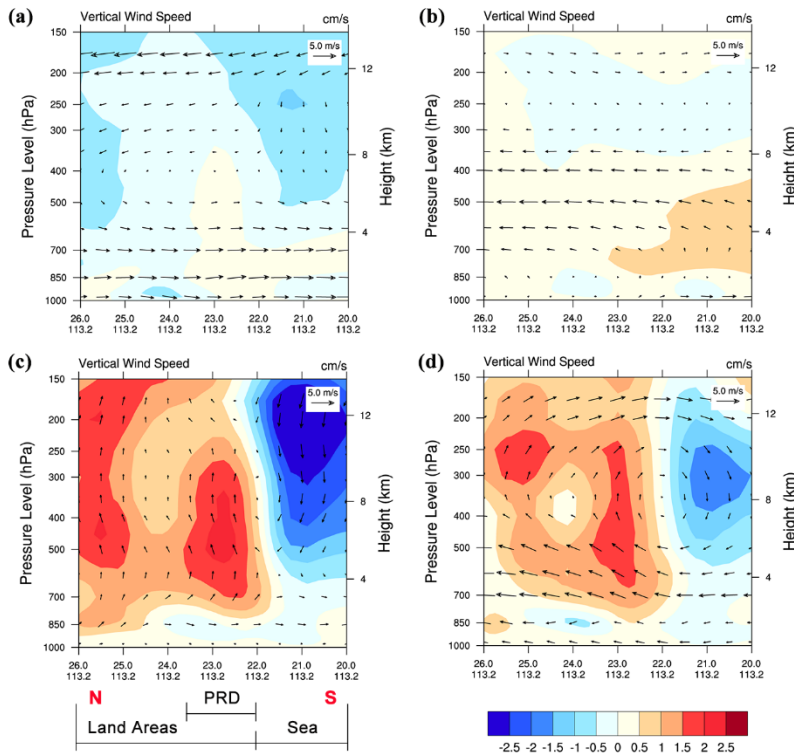
277 Downdrafts are typically considered to be an important cause of typhoon-induced O₃ pollution (Lam, 2018), but in which
278 scenarios downdrafts influence the PRD remains unclear. Thus, we explored the overall features of vertical air motions from



279 the surface layer to the tropopause in four scenarios, and the ERA-Interim reanalysis dataset (including the parameters of the
280 third category in Sect. 2.1) was utilised in the comparisons. The contours in Fig. 4 show the cross section of vertical wind
281 speed from 26.0 °N to 20.0 °N along the 113.2 °E longitude line (Fig. S4). On the typhoon-induced days in autumn, downdrafts
282 occurred over large areas above the PRD, especially above a height of ~4 km. Although updrafts can still be found near the
283 sea surface in this scenario, vertical wind speeds tended to be lower compared with those on the no-typhoon days in autumn,
284 which also suggests the enhancement of downdrafts caused by typhoons. In summer, the influence of downdrafts was found
285 over the PRD under 850 hPa on the typhoon-induced O₃ pollution days. However, overall, updrafts prevailed above the land
286 areas and downdrafts prevailed above the sea in both the typhoon-induced and no-typhoon scenarios in summer, which is
287 recognised as the structure of the East Asian summer monsoon cell (Chen et al., 1964; Jin et al., 2013; Ding et al., 2018). For
288 both updrafts and downdrafts, the absolute values of vertical wind speeds in the typhoon-induced scenario in summer were
289 overall higher than these in the corresponding no-typhoon scenario. Therefore, the approach of typhoons did not break the
290 structure of the summer monsoon cell, but rather they further strengthened the vertical motions above both land areas and sea.
291 These analyses suggest that typhoons do not necessarily lead to downdrafts during O₃ pollution periods in the PRD and its
292 adjacent areas; and in summer, vertical air motions affected by typhoons are more complicated than expected owing to the
293 existence of the East Asian summer monsoon.

294

295 We also explored the regions where downdrafts and updrafts occurred on a larger scale and their potential connections with
296 O₃ levels. As is shown in Fig. 5, though updrafts appeared in the PRD at 850 hPa on the typhoon-induced days in autumn,
297 downdrafts dominated in the region at 700 and 500 hPa. For the areas to the north of the PRD, the important role of downdrafts
298 was found at all three heights. In contrast to the no-typhoon days in autumn, downdrafts tended to cover much larger areas in
299 this scenario. Moreover, these areas at 850 and 700 hPa generally featured higher O₃ mixing ratios as well as lower RH (Fig.
300 S6) than others, which is a sign of possible direct downward O₃ transport (Roux et al., 2020; Wang et al., 2020). This part of
301 O₃ can notably aggravate near-ground O₃ pollution in the PRD. In contrast, in summer, updrafts dominated the PRD at various
302 heights in both scenarios. Besides the PRD, most of the regions near the coast were characterised by updrafts above the land
303 as well as downdrafts offshore, further indicating the ubiquity of the summer monsoon cell. By comparing the two scenarios
304 in summer, we found that typhoons resulted in more areas being influenced by updrafts. The areas with high O₃ levels did not
305 coincide with the downdraft-affected areas, and therefore, O₃ transported from the upper air may play a less significant role in
306 the typhoon-induced O₃ pollution in summer.



307

308 **Figure 4.** The cross sections of mean vertical wind field at 14:00 LT for the four scenarios: (a) autumn, typhoon-induced; (b) autumn, no-
 309 typhoon; (c) summer, typhoon-induced; and (d) summer, no-typhoon. Cross sections are from 26.0 °N to 20.0 °N along the 113.2 °E
 310 longitude line (Fig. S4). The vectors indicate meridional wind speed (m/s) and vertical wind speed (cm/s), and the contours indicate
 311 vertical wind speed (cm/s). PRD, the Pearl River Delta.

312 3.3 O₃ production conditions: comparison of clouds

313 Clouds efficiently reflect solar radiation (Liou, 1976), and therefore, they have a notable impact on the local formation of O₃.
 314 The comparison of cloud liquid water content in the cross section (Fig. 6, derived from the ERA-Interim datasets) suggests
 315 that typhoons generally resulted in fewer clouds in autumn but more clouds in summer, which agrees well with the comparison
 316 of cloud covers in Table 2. The presence of fewer clouds on the typhoon-induced days in autumn can be attributed to two
 317 reasons: the influence of dry air masses (indicated by lower RH in Table 2 and Fig. S6) and/or the hindrance of cloud formation
 318 by downdrafts. In summer, the strengthened updrafts above the land caused by typhoons favoured cloud formation, which is
 319 demonstrated by higher cloud liquid water content at the heights of 2–5 km and increases in medium and high cloud covers.
 320 In areas above the PRD below 850 hPa, downdrafts led to slight decrease of clouds in the typhoon-induced scenario in summer,
 321 which is also indicated by reduced low cloud cover. As a consequence of varied cloud covers in each scenario, on average, net
 322 surface solar radiation increased by 13% and decreased by 7% on the typhoon-induced days in autumn and summer,
 323 respectively (Table 2), which promoted and hindered O₃ production in the PRD during these two seasons, respectively.
 324

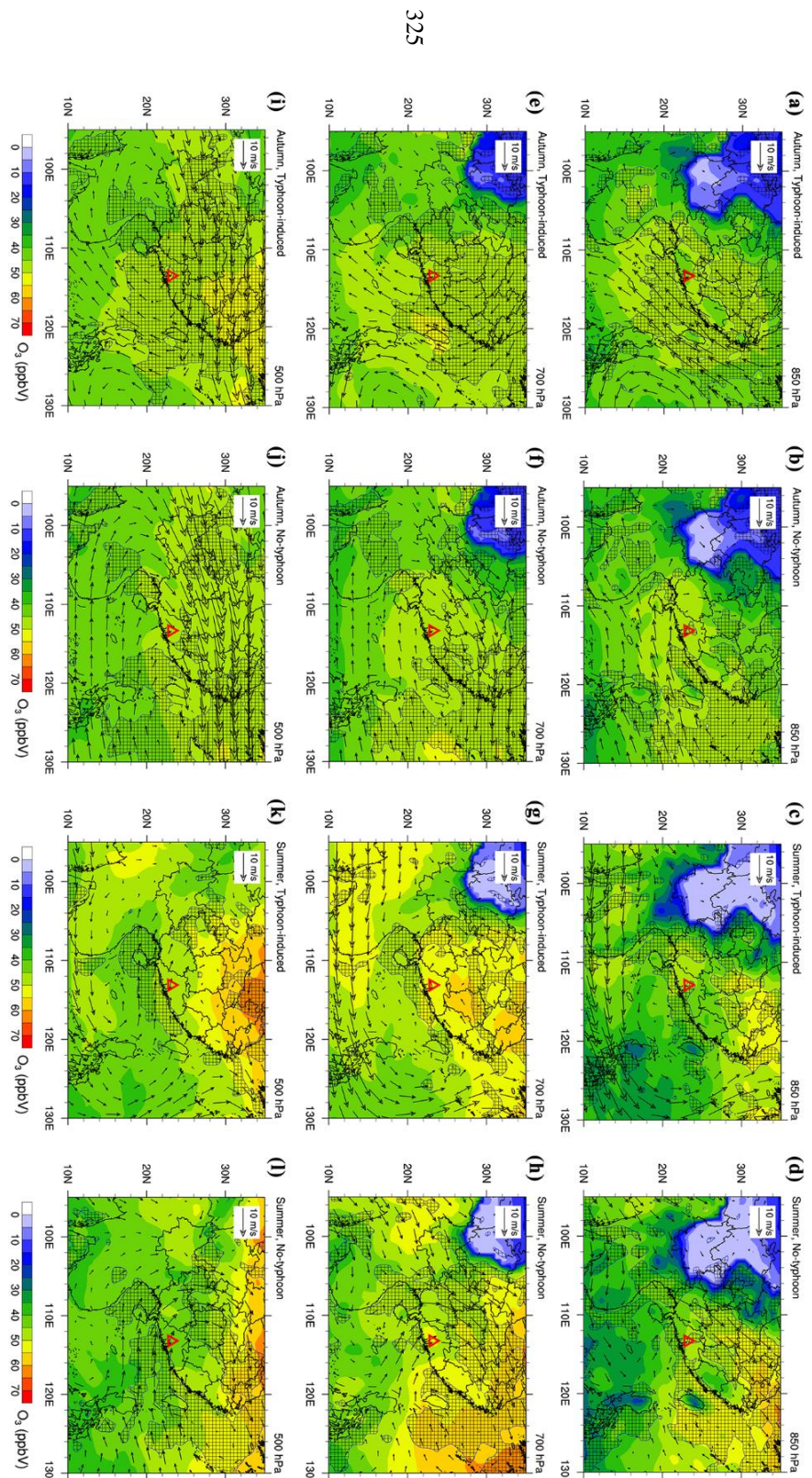
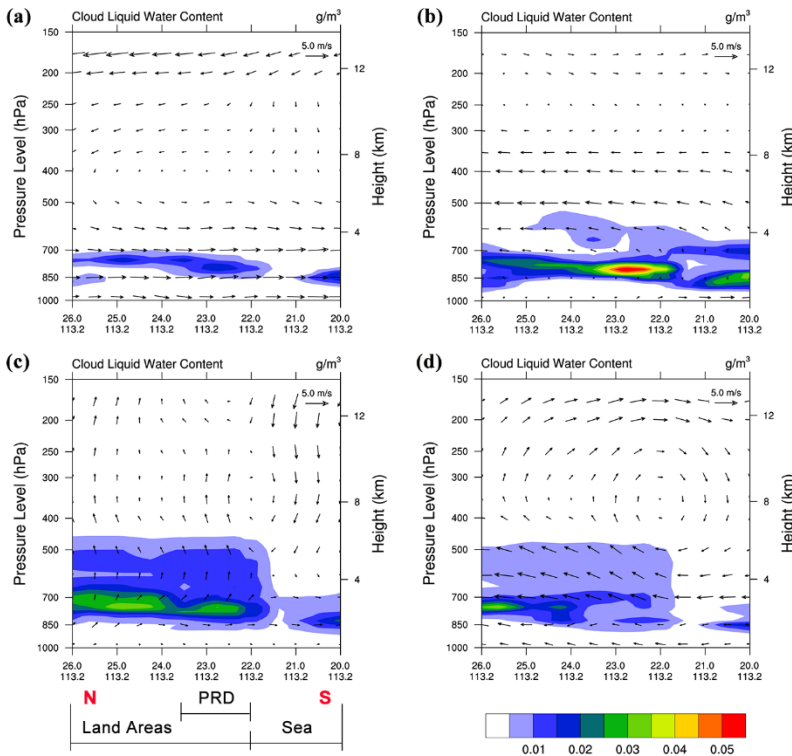


Figure 5. O₃ mixing ratio (ppbV) and wind fields at the height of (a–d) 850 hPa, (e–h) 700 hPa, and (i–l) 500 hPa at 14:00 LT for the four scenarios: (a, e, i) autumn, typhoon-induced; (b, f, j) autumn, no-typhoon; (c, g, k) summer, typhoon-induced; and (d, h, l) summer, no-typhoon. The red triangle in each plot indicates the PRD. The gridded areas indicate that vertical wind speed is less than 0, or downdrafts occur.

326
 327
 328



329

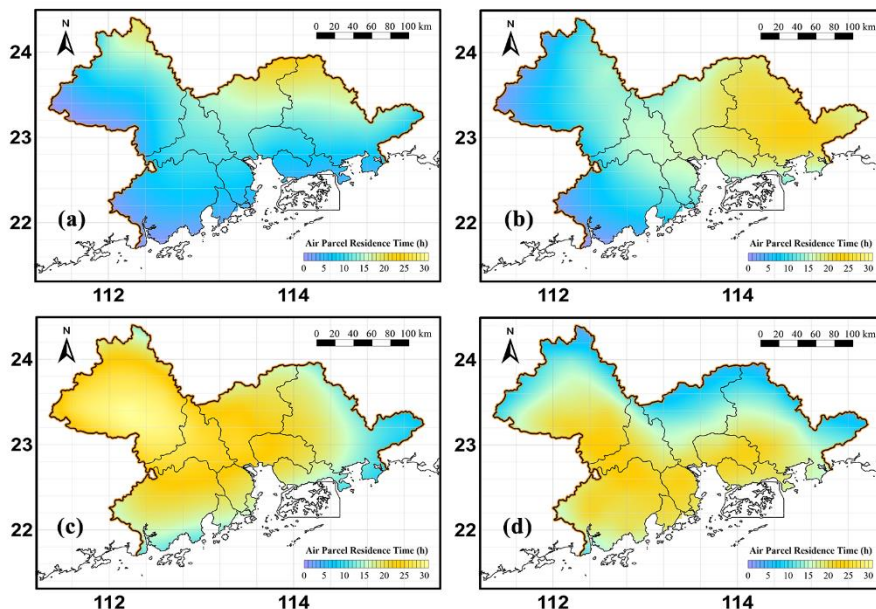
330 **Figure 6.** The cross sections of mean cloud liquid water content (g/m^3) and wind vectors at 14:00 LT for the four scenarios: (a) autumn,
 331 typhoon-induced; (b) autumn, no-typhoon; (c) summer, typhoon-induced; and (d) summer, no-typhoon. Cross sections are from 26.0 °N to
 332 20.0 °N along the 113.2 °E longitude line (Fig. S4). The vectors indicate meridional wind speed (m/s) and vertical wind speed (cm/s). PRD,
 333 the Pearl River Delta.

334 3.4 O₃ accumulation conditions: comparison of APRTs

335 The longer APRTs are, the more likely that O₃ produced by local emissions accumulates within the targeted region and notably
 336 contributes to near-ground O₃ pollution. In order to study the effect of typhoons on O₃ accumulation, we calculated APRTs in
 337 the PRD in the four scenarios (Fig. 7) for the further comparisons. On the typhoon-induced days in autumn, APRTs were
 338 typically 5–10 hours (mean = 9.5 hours) — shorter than those on the no-typhoon days in autumn (mean = 13.1 hours). In
 339 addition, lower APRT values occurred in the central part of the PRD, where high anthropogenic emissions of pollutants are
 340 distributed (Zheng et al., 2009). Despite more active O₃ chemistry discussed in the last section, locally sourced O₃ was less
 341 likely to accumulate within the PRD in this scenario, potentially limiting the contribution of local emissions for O₃. The
 342 comparison suggests opposite results in the summer scenarios, that is, APRTs on the typhoon-induced days (20–30 hours,
 343 mean = 21.0 hours) were overall higher than those on the no-typhoon days (15–25 hours, mean = 16.5 hours). This favoured
 344 the accumulation of locally sourced O₃ and offset the influence of weakened O₃ formation to some extent. In both seasons,
 345 typhoons did not cause more favourable conditions for O₃ production and accumulation simultaneously in the PRD, potentially

346 resulting in a less important role of local contributions in O₃ pollution here. More quantitative evaluations of the contributions
347 from multiple O₃ sources are discussed in Sect. 4.

348



349

350 **Figure 7.** The spatial distributions of APRTs in the PRD for the four scenarios: (a) autumn, typhoon-induced; (b) autumn, no-typhoon; (c)
351 summer, typhoon-induced; and (d) summer, no-typhoon.

352 3.5 Meteorological conditions on the close typhoon-induced days

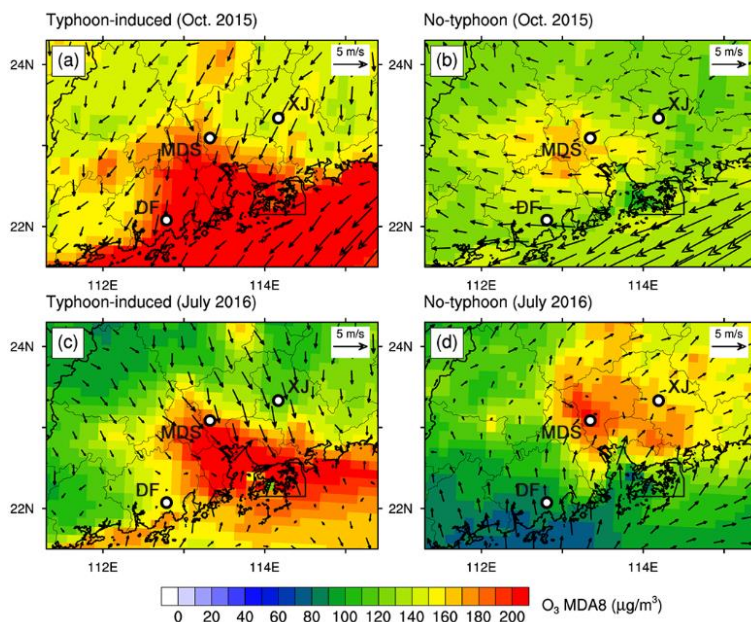
353 On the close typhoon-induced days in the two seasons, stronger north winds prevailed and total cloud cover was higher than
354 that on the no-typhoon days (Table 2), suggesting better conditions for the transport of O₃ but less favourable conditions for
355 O₃ production. As displayed in Fig. S7, the APRT values were significantly lower on the close typhoon-induced days (mean
356 = 6.6 hours, 12.9 hours in autumn and summer, respectively) than on the no-typhoon days, making it even harder for locally
357 sourced O₃ to accumulate within the PRD. Therefore, close typhoons are concluded to promote the transport of O₃ from the
358 outside and to reduce the contributions of O₃ produced from local emissions in a more notable way. In addition, close typhoons
359 led to stronger downdrafts in autumn and updrafts in summer than other scenarios in the same season (Fig. S8). It should be
360 noted that the structure of the summer monsoon cell near the PRD was destroyed in the close typhoon-induced scenario in
361 summer, indicating the stronger influence of typhoons on regional wind fields. The dominant role of O₃ transport during O₃
362 pollution days in this special scenario agrees well with the reported episode-based analyses (Lam et al., 2005; Li, 2013).



363 4 Comparisons of O₃ processes and sources

364 The comparisons of meteorological conditions served as qualitative evidence to determine the general influence of typhoons
365 on O₃ transport, production and accumulation in autumn and summer. Based on the comparison between the CMAQ modelling
366 results on typical O₃ pollution days in October 2015 and July 2016, more quantitative evidence can be presented. Figure 8
367 displays modelled mean O₃ MDA8 concentrations and wind fields (at 14:00 LT) in the four scenarios. Large standard-
368 exceedance ($> 160 \mu\text{g}/\text{m}^3$) areas were distributed in the PRD on most days, and the typhoon-induced days of both seasons
369 generally featured higher O₃ levels. The distinct wind fields for these scenarios, which were consistent with those in the longer
370 timespan (Fig. S5), indeed led to different spatial distributions of O₃. Generally, the most severe O₃ pollution occurred in the
371 downwind areas, such as the central and southern parts of the PRD on the typhoon-induced days in October 2015, the central
372 PRD on the no-typhoon days in October 2015, and the northern and eastern PRD on the no-typhoon days in July 2016. On the
373 typhoon-induced days in July 2016, high levels of O₃ accumulated around the PRE. In this section, we discuss the different
374 contributions of various O₃ processes and sources on these days to better understand the effect of typhoons on O₃ pollution in
375 the PRD.

376



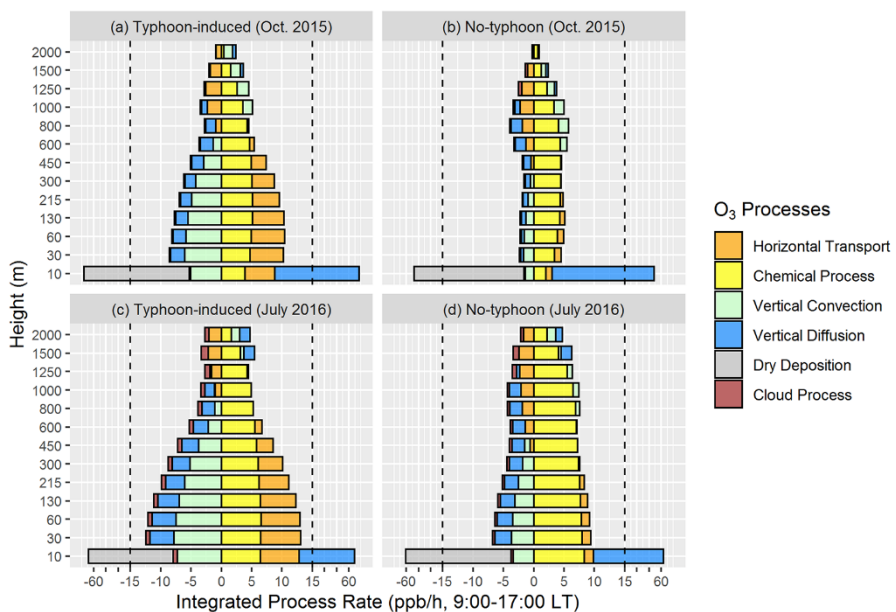
377

378 **Figure 8.** Modelling mean O₃ MDA8 concentrations ($\mu\text{g}/\text{m}^3$) and wind vectors (at 14:00 LT) on the representative O₃ pollution days: (a)
379 the typhoon-induced days in October 2015 (14–16 and 21 October 2015); (b) the no-typhoon days in October 2015 (28 October and 3–5
380 November 2015); (c) the typhoon-induced days in July 2016 (7–8 and 30–31 July 2016); and (d) the no-typhoon days in July 2016 (22–26
381 and 29 July 2016). Three representative sites in the PRD are shown as black circles in the plots: XJ, Xijiao; MDS, Modiesha; DF,
382 Duanfen.

383 **4.1 O₃ processes: transport vs chemical process**

384 The PA tool in CMAQ was used to quantify the contributions of transport and chemical process to the O₃ variations on O₃
385 pollution days under various scenarios in October 2015 and July 2016. As is shown in Fig. 9, the daytime (9:00–17:00 LT) O₃
386 PA results within the PRD in all scenarios share similar characteristics. Dry deposition dominated O₃ removal near the surface,
387 and it also led to high gradients of O₃ concentrations that promote downward O₃ diffusion. Within the PBL (about 0–1 km in
388 height), O₃ was mainly contributed by horizontal transport and chemical process, and vertical convection led to the drop of O₃
389 concentrations. However, differences existed between the O₃ PA results in four scenarios, indicating the impact of typhoons
390 on the transport and production of O₃. In both months, typhoons led to notably higher contribution of horizontal transport to
391 O₃, especially in the lower and middle part of the PBL. Within the PBL, on average, it increased from -0.9 ppb/h, -0.8 ppb/h
392 to 1.2 ppb/h, 2.0 ppb/h under typhoon influence in autumn and summer, respectively. The comparison of the contribution of
393 chemical process (in absolute rates) suggests that they had opposite effects in the two months — under typhoons, the
394 contribution increased in October 2015 (from 4.0 ppb/h to 4.5 ppb/h within the PBL, or by 11.4%), but it decreased in July
395 2016 (from 7.1 ppb/h to 5.7 ppb/h within the PBL, or by -20.8%). In other words, typhoons promoted and hindered O₃
396 production in autumn and summer, respectively. These results agree well with the comparisons of O₃ transport and production
397 conditions in the previous section.

398



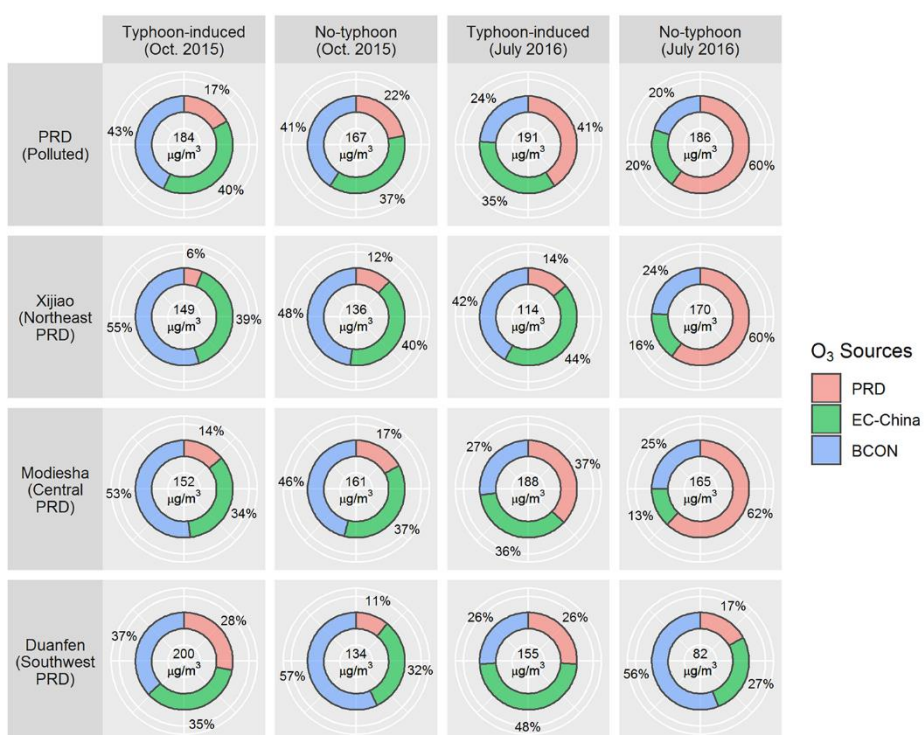
399

400 **Figure 9.** The daytime-mean (9:00–17:00 LT) hourly contributions of O₃ processes within the PRD in vertical layers 1–13 on representative O₃
401 pollution days: (a) the typhoon-induced days in October 2015 (14–16 and 21 October 2015); (b) the no-typhoon days in October 2015
402 (28 October and 3–5 November 2015); (c) the typhoon-induced days in July 2016 (7–8 and 30–31 July 2016); and (d) the no-typhoon days
403 in July 2016 (22–26 and 29 July 2016).



404 4.2 O₃ sources: local sources vs regional sources

405 The contributions of various sources to O₃ within the PRD are determined by the combined impact of O₃ transport, production
406 and accumulation. The results for the daytime (9:00–17:00 LT) O₃ SA near the ground (about 0–80 m in height) in four
407 scenarios are illustrated in Fig. 10. For polluted regions within the PRD, stronger O₃ production under typhoons did not lead
408 to a higher proportion of local contributions to O₃ pollution in October 2015 — it even decreased from 22% (on the no-typhoon
409 days) to 17% (on the typhoon-induced days). The contributions of EC-China emissions and BCON, in contrast, increased
410 slightly from 37%, 41% to 40%, 43%, respectively. The distinction of the O₃ SA results is more apparent for the summer
411 scenarios, that is, typhoons resulted in growing contributions from O₃ transported from other regions (from 40% to 59%) but
412 decreased local contributions (from 60% to 41%) in July 2016. More favourable O₃ accumulation conditions (indicated by
413 higher APRTs on the representative typhoon-induced O₃ pollution days in summer (Fig. S9)) were far from sufficient to
414 compensate for the effect of weakened O₃ production on the high contributions of local sources.
415



416

417 **Figure 10.** The O₃ SA near the ground (about 0–80 m in height) on representative O₃ pollution days for the four scenarios (the average
418 results of 9:00–17:00 LT). The locations of the three representative sites (Xijiao, Modiesha and Duanfen) are shown in Fig. 8. PRD, the
419 Pearl River Delta; EC-China, East China and Central China; BCON, the boundary conditions of the d02 modelling.

420 Furthermore, owing to the variations of wind fields, the comparison results of O₃ SA in different parts of the PRD may differ
421 from the regional ones. For instance, while the comparisons of O₃ SA in the Xijiao and Modiesha site (located in the northeast



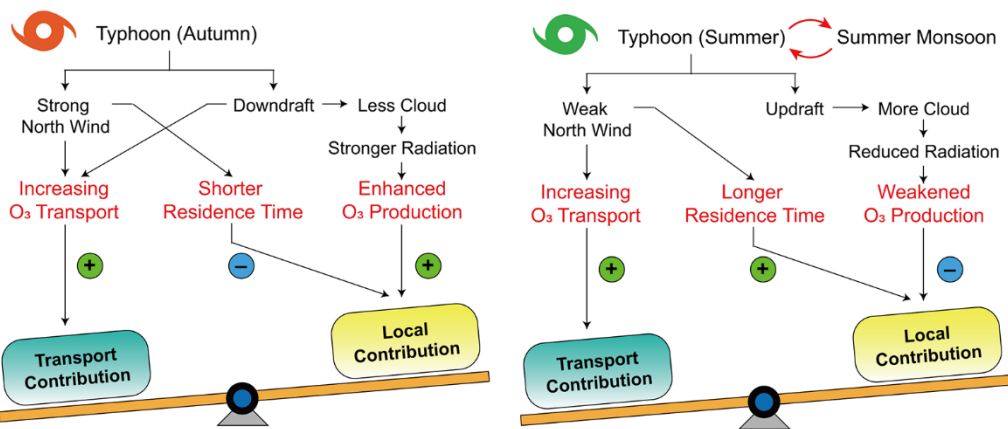
422 and central part of the PRD, respectively) agree well with those in the polluted regions of the PRD, higher contributions of
423 PRD emissions for O₃ can be found in the Duanfen site (located in the southwest part of the PRD) on the typhoon-induced
424 days of two months in comparison to these on the corresponding no-typhoon days (Fig. 10). Since the site was located in the
425 downwind region in the typhoon-induced scenario in October 2015 (Fig. 8a), enhanced O₃ production led by typhoons from
426 the massive emissions of O₃ precursors in the central PRD (Zheng et al., 2009) contributed to higher local contributions for O₃
427 pollution here (the highest local contribution in the PRD occurred in areas near the Duanfen site and almost reached 40% in
428 this scenario, which was even higher than that in the corresponding no-typhoon scenario (33%)). In the no-typhoon scenario
429 in July 2016, the site was located in the upwind regions under the prevailing of southwest winds, limiting the contributions of
430 local emissions for O₃ at the site (Fig. 8d). Thus, higher local contributions can also be found in the typhoon-induced scenario
431 in this month.

432 5 Discussion and conclusions

433 The significance of typhoons on O₃ pollution in the PRD calls for thorough evaluations of the different causes of O₃ pollution
434 with the appearance of typhoons in the Northwest Pacific. In this study, we revealed the different impacts of typhoons on O₃
435 transport, production and accumulation in the PRD (as summarised in Fig. 11) through systematic comparisons of
436 meteorological conditions, the contributions of various O₃ processes and sources in the typhoon-induced and no-typhoon
437 scenarios. We found that typhoons tended to promote O₃ transport towards the PRD, but failed to provide more favourable O₃
438 production and accumulation conditions simultaneously, which limited the contribution of local emissions to O₃ pollution.
439 Furthermore, there were also differences between the influence of typhoons on O₃ pollution in autumn and summer. More
440 favourable transport conditions occurred in the typhoon-induced scenario in autumn, which was characterised by higher wind
441 speeds and the increased influence of downdrafts. In summer, the mixed types of air masses in the typhoon-induced scenario
442 were likely to bring more O₃ into the PRD than the clean marine air masses in the no-typhoon scenario, also suggesting
443 enhanced O₃ transport under the influence of typhoons. Generally, typhoons led to cloudless conditions, stronger solar radiation,
444 and thus more rapid O₃ production in autumn, but shorter APRTs (5–10 hours) suggest that locally sourced O₃ was hard to
445 accumulate within the PRD. As a result, the contributions in percentage of local emissions to O₃ pollution decreased (slightly
446 by ~5% for the polluted regions of the PRD in October 2015). In contrast, in summer, intensified updrafts associated with
447 typhoons strengthened cloud formation, weakened solar radiation, and thus restrained local O₃ production. Longer APRTs (>
448 20 hour) under typhoon influence were far from sufficient to maintain high contributions of local emissions for O₃ pollution
449 (which decreased by ~20% for the polluted regions of the PRD in July 2016). However, due to the variations of wind fields
450 under different scenarios, the changes of local and transport contributions for O₃ led by typhoons were different in the
451 southwest part of the PRD, that is, higher contribution from emissions within the PRD and reduced transport contribution
452 occurred in the typhoon-induced scenarios in both seasons. As for the close typhoon-induced scenario, O₃ transport was further

453 strengthened, but meteorological conditions in the PRD became less favourable for both the production and accumulation of
454 O₃.

455



456

457 **Figure 11.** The summary of the causes of O₃ pollution in the PRD under typhoon influence in autumn and summer.

458 The East Asian monsoon, changing with seasons, has a pronounced impact on local meteorological conditions as well as the
459 characteristics of O₃ pollution in East China (He et al., 2008). The seasonal behaviour of the East Asian monsoon is likely to
460 result in the seasonally varied effect of typhoons on O₃ pollution in the PRD. In October, the summer monsoon has almost
461 finished its retraction and the winter monsoon is beginning (Ding, 1994). Thus, there are not many obstacles to the southward
462 movement of typhoon periphery and the transport of O₃ towards the PRD by the continental and coastal air masses. Large
463 downdraft-influenced areas in Central and South China occur in this scenario, and high O₃ levels and low RH in these areas
464 indicate the potentially important role of directly downward O₃ transport. In July, the summer monsoon reaches its strongest
465 (Ding, 1994). The interaction between typhoon periphery and the summer monsoon results in stagnation and enhanced updrafts
466 above the land areas of the PRD and its surroundings. Only when typhoon is close enough to the PRD is the stagnation
467 terminated and the structure of the summer monsoon cell broken. This also explains why some summertime typhoon-induced
468 O₃ episodes in the PRD can be typically divided into two periods, as stagnation leads to the accumulation of locally produced
469 O₃ in the first phase and strong northerly winds strengthen O₃ transport before the landing of typhoons (Lam et al., 2005; Li,
470 2013). It should be noted that updrafts, rather than downdrafts, prevailed on the typhoon-induced O₃ pollution days in summer.
471 High levels of O₃ did not necessarily occur in the regions dominated by downdrafts in this scenario, suggesting a less notable
472 connection between downdrafts and summertime O₃ pollution in the PRD. Further investigations are required to trace the
473 detailed process of downward O₃ transport, including the stratosphere-troposphere exchange (Stohl et al., 2003), in each
474 scenario, and quantify their contributions to near-ground O₃ pollution.

475



476 Some limitations remain in this study. We chose O₃ pollution days as individual samples, ignoring the influence of O₃ pollution
477 on the previous days. Thus, more detailed full-episode analyses are required. Moreover, owing to the small sampling size, the
478 influence of typhoons on O₃ pollution in the PRD is still not fully understood, including, for instance, the detailed connections
479 between the features of typhoons (intensity, position) and O₃ pollution. However, the comparisons of meteorological conditions,
480 O₃ processes and sources in different scenarios and seasons demonstrate the complex causes of typhoon-induced O₃ pollution
481 in the PRD — typhoons tend to enhance O₃ transport into the PRD in both seasons, but their impacts on the production and
482 accumulation of O₃ are completely different. As a result, emissions within (outside of) the PRD are likely to contribute less
483 (more) on the typhoon-induced O₃ pollution days than on the no-typhoon days, and more attention should be paid to controlling
484 anthropogenic emissions of O₃ precursors on a larger scale under typhoon influence. This study also suggests that a thorough
485 evaluation of O₃ transport, production and accumulation conditions can be applied to understand the causes of regional O₃
486 pollution not only in the PRD, but also in other regions.

487

488 *Data availability.* Data are available from the corresponding author upon request.

489

490 *Author contributions.* KQ, XW and YZ designed the study. KQ, XW, and TX did the simulation work, including the operation
491 of the WRF, SMOKE and CMAQ models. JS, HD, LZ and YZ provided observational results of field campaigns and the
492 routine monitoring datasets for the evaluation of model performance. KQ, XW, YY and YZ analysed the modelling results.
493 KQ, XW, YY and YZ wrote and revised this paper, with critical feedbacks from all other authors.

494

495 *Competing interests.* The authors declare no conflict of interest.

496

497 *Acknowledgements.* This work was supported by the National Key Research and Development Program of China (Grant No.
498 2018YFC0213204, 2018YFC0213506) and the National Science and Technology Pillar Program of China (Grant No.
499 2014BAC21B01).

500



501 **References**

- 502 Berrisford, P., Dee, D., Poli, P., Brugge, R., Fielding, K., Fuentes, M., Kallberg, P., Kobayashi, S., Uppala, S., and Simmons,
503 A.: The ERA-Interim archive Version 2.0, ERA report series, 1, 1–16, 2011.
- 504 Carter, W. P. L.: Development of the SAPRC-07 chemical mechanism, *Atmos. Environ.*, 44, 5324–5335,
505 <https://doi.org/10.1016/j.atmosenv.2010.01.026>, 2010.
- 506 Chen, H., Wang, X., Shen, J., Lu, K., and Zhang, Y.: Ozone source apportionment of typical photochemical pollution
507 episodes in the Pearl River Delta in autumn, *Acta Scientiarum Naturalium Universitatis Pekinensis* (in Chinese), 51,
508 620–630, <https://doi.org/10.13209/j.0479-8023.2015.089>, 2015.
- 509 Chen, Q., Miao, J., and Li, W.: A comparison of mean wind field and mean meridional circulation between south-west
510 monsoon area in Southeast Asia and Pacific trade wind area in July, 1958, *Acta Meteorologica Sinica* (in Chinese),
511 34(1), 51–61, <https://doi.org/10.11676/qxxb1964.006>, 1964.
- 512 Chen, X., Liu, Y., Lai, A., Han, S., Fan, Q., Wang, X., Ling, Z., Huang, F., and Fan, S.: Factors dominating 3-dimensional
513 ozone distribution during high tropospheric ozone period, *Environ. Pollut.*, 232, 55–64,
514 <https://doi.org/10.1016/j.envpol.2017.09.017>, 2018.
- 515 Chow, E. C., Li, R. C., and Zhou, W.: Influence of tropical cyclones on Hong Kong air quality, *Adv. Atmos. Sci.*, 35(9),
516 1177–1188, <https://doi.org/10.1007/s00376-018-7225-4>, 2018.
- 517 Chow, E. C., Wen, M., Li, L., Leung, M. Y., Cheung, P. K., and Zhou, W.: Assessment of the Environmental and Societal
518 Impacts of the Category-3 Typhoon Hato, *Atmosphere*, 10(6), 296. <https://doi.org/10.3390/atmos10060296>, 2019.
- 519 Clappier, A., Belis, C. A., Pernigotti, D., and Thunis, P.: Source apportionment and sensitivity analysis: two methodologies
520 with two different purposes, *Geosci. Model Dev.*, 10, 4245–4256, <https://doi.org/10.5194/gmd-10-4245-2017>, 2017.
- 521 Dee, D. P., Uppala, S. M., Simmons, A. J., Berrisford, P., Poli, P., Kobayashi, S., Andrae, U., Balmaseda, M. A., Balsamo,
522 G., Bauer, P., Bechtold, P., Beijaaars, A.C.M., van de Berg, L., Bidiot, J., Bormann, N., Delsol, C., Dragani, R., Fuentes,
523 M., Geer, A.J., Haimberger, L., Healy, S.B., Hersbach, H., H ölm, E.V., Isaksen, L., Isaksen, L., K ålberg, P., K öhler,
524 M., Matricardi, M., McNally, A.P., Monge-Sanz, B.M., Morcrette, J.-J., Park, B.-K., Peubey, C., de Rosnay, P.,
525 Tavolato, Th épaut, J.-N., and Vitart, F.: The ERA-Interim reanalysis: Configuration and performance of the data
526 assimilation system, *Q. J. Roy. Meteor. Soc.*, 137(656), 553–597, <https://doi.org/10.1002/qj.828>, 2011.
- 527 Deng, T., Wang, T., Wang, S., Zou, Y., Yin, C., Li, F., Liu, L., Wang, N., Song, L., Wu, C., and Wu, D.: Impact of typhoon
528 periphery on high ozone and high aerosol pollution in the Pearl River Delta region, *Sci. Total Environ.*, 668, 617–630,
529 <https://doi.org/10.1016/j.scitotenv.2019.02.450>, 2019.
- 530 Ding, Y. H.: Monsoons over China, Kluwer Academic Publishers, Dordrecht/Boston/London, 1994.
- 531 Ding, Y., Si, D., Liu, Y., Wang, Z., Li, Y., Zhao, L., and Song, Y.: On the Characteristics, Driving Forces and Inter-decadal
532 Variability of the East Asian Summer Monsoon, *Chinese Journal of Atmospheric Sciences* (in Chinese), 42(3), 533–
533 558, <https://doi.org/10.3878/j.issn.1006-9895.1712.17261>, 2018.



- 534 Feng, Y., Ning, M., Lei, Y., Sun, Y., Liu, W., and Wang, J.: Defending blue sky in China: Effectiveness of the “Air
535 Pollution Prevention and Control Action Plan” on air quality improvements from 2013 to 2017, *J. Environ. Manage.*,
536 252, 109603, <https://doi.org/10.1016/j.jenvman.2019.109603>, 2019.
- 537 Gao, X., Deng, X., Tan, H., Wang, C., Wang, N., and Yue, D.: Characteristics and analysis on regional pollution process and
538 circulation weather types over Guangdong Province, *Acta Scientiae Circumstantiae* (in Chinese), 38(5), 1708–1716,
539 <https://doi.org/10.13671/j.hjkxxb.2017.0473>, 2018.
- 540 Guo, J., Miao, Y., Zhang, Y., Liu, H., Li, Z., Zhang, W., He, J., Lou, M., Yan, Y., Bian, L., and Zhai, P.: The climatology of
541 planetary boundary layer height in China derived from radiosonde and reanalysis data, *Atmos. Chem. Phys.*, 16, 13309–
542 13319, <https://doi.org/10.5194/acp-16-13309-2016>, 2016.
- 543 He, K.: Multi-resolution Emission Inventory for China (MEIC): model framework and 1990–2010 anthropogenic emissions,
544 American Geophysical Union, Fall Meeting 2012, San Francisco, the United States of America, 3–7 December 2012,
545 A32B-05, 2012.
- 546 He, Y. J., Uno, I., Wang, Z. F., Pochanart, P., Li, J., and Akimoto, H.: Significant impact of the East Asia monsoon on ozone
547 seasonal behavior in the boundary layer of Eastern China and the west Pacific region, *Atmos. Chem. Phys.*, 8, 7543–
548 7555, <https://doi.org/10.5194/acp-8-7543-2008>, 2008.
- 549 Huang, J. P., Fung, J. C., Lau, A. K., and Qin, Y.: Numerical simulation and process analysis of typhoon-related ozone
550 episodes in Hong Kong, *J. Geophys. Res.-Atmos.*, 110(D5), <https://doi.org/10.1029/2004JD004914>, 2005.
- 551 Huang, Y., Yao, T., Fung, J. C., Lu, X., and Lau, A. K.: Application of air parcel residence time analysis for air pollution
552 prevention and control policy in the Pearl River Delta region, *Sci. Total Environ.*, 658, 744–752,
553 <https://doi.org/10.1016/j.scitotenv.2018.12.205>, 2019.
- 554 Jin, Q., Yang, X. Q., Sun, X. G., and Fang, J. B.: East Asian summer monsoon circulation structure controlled by feedback
555 of condensational heating, *Clim. Dynam.*, 41(7–8), 1885–1897, <https://doi.org/10.1007/s00382-012-1620-9>, 2013.
- 556 Jiang, F., Wang, T., Wang, T., Xie, M., and Zhao, H.: Numerical modeling of a continuous photochemical pollution episode
557 in Hong Kong using WRF-chem, *Atmos. Environ.*, 42(38), 8717–8727,
558 <https://doi.org/10.1016/j.atmosenv.2008.08.034>, 2008.
- 559 Lam, K. S., Wang, T. J., Wu, C. L., and Li, Y. S.: Study on an ozone episode in hot season in Hong Kong and transboundary
560 air pollution over Pearl River Delta region of China, *Atmos. Environ.*, 39(11), 1967–1977,
561 <https://doi.org/10.1016/j.atmosenv.2004.11.023>, 2005.
- 562 Lam, Y. F.: Climate change and air quality in Southeastern China: Hong Kong study, in: Climate change and air pollution,
563 edited by: Akhtar R., and Palagiano C., Springer, Cham, 181–196, https://doi.org/10.1007/978-3-319-61346-8_12,
564 2018.
- 565 Lam, Y. F., Cheung, H. M., and Ying, C. C.: Impact of tropical cyclone track change on regional air quality, *Sci. Total
566 Environ.*, 610, 1347–1355, <https://doi.org/10.1016/j.scitotenv.2017.08.100>, 2018.



- 567 Li, J., Lu, K., Lv, W., Li, J., Zhong, L., Ou, Y., Chen, D., Huang, X., and Zhang, Y.: Fast increasing of surface ozone
568 concentrations in Pearl River Delta characterized by a regional air quality monitoring network during 2006–2011, *J.
569 Environ. Sci.*, 26(1), 23–36, [https://doi.org/10.1016/S1001-0742\(13\)60377-0](https://doi.org/10.1016/S1001-0742(13)60377-0), 2014.
- 570 Li, M., Jiang, S., Gan, Q., Chen, F., Zeng, D., Li, J., Fan, S., and Zhu, W.: Characteristics of ozone pollution and analysis of
571 typical pollution processes in summer and autumn in Huizhou, *Acta Scientiarum Naturalium Universitatis Sunyatseni*
572 (in Chinese), 57(5), 29, <https://doi.org/10.13471/j.cnki.acta.snus.2018.05.004>, 2018.
- 573 Li, M., Zhang, Q., Kurokawa, J.-I., Woo, J.-H., He, K., Lu, Z., Ohara, T., Song, Y., Streets, D. G., Carmichael, G. R., Cheng,
574 Y., Hong, C., Huo, H., Jiang, X., Kang, S., Liu, F., Su, H., and Zheng, B.: MIX: a mosaic Asian anthropogenic emission
575 inventory under the international collaboration framework of the MICS-Asia and HTAP, *Atmos. Chem. Phys.*, 17, 935–
576 963, <https://doi.org/10.5194/acp-17-935-2017>, 2017.
- 577 Li, K., Jacob, D. J., Liao, H., Shen, L., Zhang, Q., and Bates, K. H.: Anthropogenic drivers of 2013–2017 trends in summer
578 surface ozone in China, *P. Natl. Acad. Sci. USA*, 116(2), 422–427, <https://doi.org/10.1073/pnas.1812168116>, 2019.
- 579 Li, Y.: The evolution characteristics and source analysis of the secondary pollutants in summer over Pearl River Delta, Ph.D.
580 thesis, College of Environmental Science and Engineering, Peking University, China, 160 pp., 2013.
- 581 Li, Y., Lau, A. K. H., Fung, J. C. H., Zheng, J.Y., Zhong, L. J., and Louie, P. K. K.: Ozone source apportionment (OSAT) to
582 differentiate local regional and super-regional source contributions in the Pearl River Delta region, China, *J. Geophys.
583 Res.-Atmos.*, 117, D15305, <http://doi.org/10.1029/2011JD017340>, 2012.
- 584 Liou, K. N.: On the absorption, reflection and transmission of solar radiation in cloudy atmospheres, *J. Atmos. Sci.*, 33(5),
585 798–805, [https://doi.org/10.1175/1520-0469\(1976\)033<0798:OTARAT>2.0.CO;2](https://doi.org/10.1175/1520-0469(1976)033<0798:OTARAT>2.0.CO;2), 1976.
- 586 Lin, X., Yuan, Z., Yang, L., Luo, H., and Li, W.: Impact of extreme meteorological events on ozone in the Pearl River Delta,
587 China, *Aerosol Air Qual. Res.*, 19(6), 1307–1324, <https://doi.org/10.4209/aaqr.2019.01.0027>, 2019.
- 588 Liu, H., Liu, S., Xue, B., Lv, Z., Meng, Z., Yang, X., Xue, T., Yu, Q., and He, K.: Ground-level ozone pollution and its
589 health impacts in China, *Atmos. Environ.*, 173, 223–230, <https://doi.org/10.1016/j.atmosenv.2017.11.014>, 2018.
- 590 Lu, X., Hong, J., Zhang, L., Cooper, O. R., Schultz, M. G., Xu, X., Wang, T., Gao, M., Zhao, Y., and Zhang, Y.: Severe
591 surface ozone pollution in China: A global perspective, *Environ. Sci. Tech. Lett.*, 5(8), 487–494,
592 <https://doi.org/10.1021/acs.estlett.8b00366>, 2018.
- 593 Mills, G., Sharps, K., Simpson, D., Pleijel, H., Broberg, M., Uddling, J., Jaramillo, F., Davies, W. J., Dentener, F., Van den
594 Berg, M., Agrawal, M., Agrawal, S. B., Ainsworth, E. A., Bäker, P., Emberson, L., Feng, Z., Harmens, H., Hayes, F.,
595 Kobayashi, K., Paoletti, E., and Van Dingenen, R.: Ozone pollution will compromise efforts to increase global wheat
596 production, *Glob. Change Biol.*, 24, 3560–3574, <https://doi.org/10.1111/gcb.14157>, 2018.
- 597 National Research Council: Rethinking the Ozone Problem in Urban and Regional Air Pollution, *Natl. Acad. Press*,
598 Washington, D. C., USA, 1991.



- 599 Roux, F., Clark, H., Wang, K.-Y., Rohs, S., Sauvage, B., and Néeldec, P.: The influence of typhoons on atmospheric
600 composition deduced from IAGOS measurements over Taipei, *Atmos. Chem. Phys.*, 20, 3945–3963,
601 <https://doi.org/10.5194/acp-20-3945-2020>, 2020.
- 602 So, K. L. and Wang, T.: On the local and regional influence on ground-level ozone concentrations in Hong Kong, *Environ.
603 Pollut.*, 123(2), 307–317, [https://doi.org/10.1016/S0269-7491\(02\)00370-6](https://doi.org/10.1016/S0269-7491(02)00370-6), 2003.
- 604 Stein, A. F., Draxler, R. R., Rolph, G. D., Stunder, B. J., Cohen, M. D., and Ngan, F.: NOAA's HYSPLIT atmospheric
605 transport and dispersion modeling system, *B. Am. Meteorol. Soc.*, 96(12), 2059–2077, <https://doi.org/10.1175/BAMS-D-14-00110.1>, 2015.
- 606 Stohl, A., Bonasoni, P., Cristofanelli, P., Collins, W., Feichter, J., Frank, A., Forster, C., Gerasopoulos, E., Gaggeler, H.,
607 James, P., Kentarchos, T., Kromp-Kolb, H., Kruger, B., Land, C., Meloen, J., Papayannis, A., Priller, A., Seibert, P.,
608 Sprenger, M., Roelofs, G. J., Scheel, H. E., Schnabel, C., Siegmund, P., Tobler, L., Trickl, T., Wernli, H., Wirth, V.,
609 Zanis, P., and Zerefos, C.: Stratosphere-troposphere exchange: A review, and what we have learned from STACCATO,
610 *J. Geophys. Res.*, 108, 8516, <https://doi.org/10.1029/2002JD002490>, 2003.
- 611 Wang, H., Wang, W., Huang, X., and Ding A.: Impacts of stratosphere-to-troposphere-transport on summertime surface
612 ozone over eastern China, *Sci. Bull.*, 65, 276–279, <https://doi.org/10.1016/j.scib.2019.11.017>, 2020.
- 613 Wang, N., Guo, H., Jiang, F., Ling, Z. H., and Wang, T.: Simulation of ozone formation at different elevations in
614 mountainous area of Hong Kong using WRF-CMAQ model, *Sci. Total Environ.*, 505, 939–951,
615 <https://doi.org/10.1016/j.scitotenv.2014.10.070>, 2015.
- 616 Wang, T. and Kwok, J. Y.: Measurement and analysis of a multiday photochemical smog episode in the Pearl River Delta of
617 China, *J. Appl. Meteorol.*, 42(3), 404–416, [https://doi.org/10.1175/1520-0450\(2003\)042<0404:MAAOAM>2.0.CO;2](https://doi.org/10.1175/1520-0450(2003)042<0404:MAAOAM>2.0.CO;2), 2003.
- 618 Wang, T., Lam, K. S., Lee, A. S., Pang, S. W., and Tsui, W. S.: Meteorological and chemical characteristics of the
619 photochemical ozone episodes observed at Cape D'Aguilar in Hong Kong, *J. Appl. Meteorol.*, 37(10), 1167–1178,
620 [https://doi.org/10.1175/1520-0450\(1998\)037<1167:MACCOT>2.0.CO;2](https://doi.org/10.1175/1520-0450(1998)037<1167:MACCOT>2.0.CO;2), 1998.
- 621 Wang, T., Wu, Y. Y., Cheung, T. F., and Lam, K. S.: A study of surface ozone and the relation to complex wind flow in
622 Hong Kong, *Atmos. Environ.*, 35(18), 3203–3215, [https://doi.org/10.1016/S1352-2310\(00\)00558-6](https://doi.org/10.1016/S1352-2310(00)00558-6), 2001.
- 623 Wang, T., Xue, L., Brimblecombe, P., Lam, Y. F., Li, L., and Zhang, L.: Ozone pollution in China: A review of
624 concentrations, meteorological influences, chemical precursors, and effects, *Sci. Total Environ.*, 575, 1582–1596,
625 <https://doi.org/10.1016/j.scitotenv.2016.10.081>, 2017.
- 626 Wang, X., Zhang, Y., Hu, Y., Zhou, W., Lu, K., Zhong, L., Zeng, L., Shao, M., Hu, M., and Russell, A. G.: Process analysis
627 and sensitivity study of regional ozone formation over the Pearl River Delta, China, during the PRIDE-PRD2004
628 campaign using the Community Multiscale Air Quality modeling system, *Atmos. Chem. Phys.*, 10, 4423–4437,
629 <https://doi.org/10.5194/acp-10-4423-2010>, 2010.
- 630
- 631



- 632 Wei, X., Lam, K. S., Cao, C., Li, H., and He, J.: Dynamics of the typhoon Haitang related high ozone episode over Hong
633 Kong, *Adv. Meteorol.*, 2016, <https://doi.org/10.1155/2016/6089154>, 2016.
- 634 Yang, J. X., Lau, A. K. H., Fung, J. C. H., Zhou, W., and Wenig, M.: An air pollution episode and its formation mechanism
635 during the tropical cyclone Nuri's landfall in a coastal city of south China, *Atmos. Environ.*, 54, 746–753,
636 <https://doi.org/10.1016/j.atmosenv.2011.12.023>, 2012.
- 637 Ying, M., Zhang, W., Yu, H., Lu, X., Feng, J., Fan, Y., Zhu, Y., and Chen, D.: An overview of the China Meteorological
638 Administration tropical cyclone database, *J. Atmos. Ocean Tech.*, 31(2), 287–301, <https://doi.org/10.1175/JTECH-D-12-00119.1>, 2014.
- 640 Yue, H., Gu, T., Wang, C., Wu, D., Deng, X., Huang, J., and Wang, Y.: Influence of typhoon Nida process on ozone
641 concentration in Guangzhou, *Acta Scientiae Circumstantiae* (in Chinese), 38(12), 4565–4572,
642 <https://doi.org/10.13671/j.hjkxxb.2018.0319>, 2018.
- 643 Zhang, X., Liu, Y., Deng, X., Chen, P., Feng, Y., and Fan, Q.: Analysis of summertime typical pollution in Pearl River Delta
644 region—numerical simulation of meteorological field, *Meteorological and Environmental Research*, 59(4), 9–18,
645 2014.
- 646 Zhao, W., Gao, B., Liu, M., Lu, Q., Ma, S., Sun, S., Sun, J., Chen, L., and Fan, S.: Impact of meteorological factors on the
647 ozone pollution in Hong Kong, *Huan jing ke xue= Huanjing kexue* (in Chinese), 40(1), 55–66,
648 <https://doi.org/10.13227/j.hjkx.201803151>, 2019.
- 649 Zheng, J., Zhang, L., Che, W., Zheng, Z., and Yin, S.: A highly resolved temporal and spatial air pollutant emission
650 inventory for the Pearl River Delta region, China and its uncertainty assessment, *Atmos. Environ.*, 43(32), 5112–5122,
651 <https://doi.org/10.1016/j.atmosenv.2009.04.060>, 2009.
- 652 Zheng, J., Zhong, L., Wang, T., Louie, P. K. K., and Li, Z.: Ground-level ozone in the Pearl River Delta region: Analysis of
653 data from a recently established regional air quality monitoring network, *Atmos. Environ.*, 44(6), 814–823,
654 <https://doi.org/10.1016/j.atmosenv.2009.11.032>, 2010.